Leveraging CRISPR-Cas13d in an inducible knockdown system to interrogate *Drosophila* germ granule mRNAs

Zoya A. Gauhar[1], Cameron Myhrvold[1,2,3,4*], and Elizabeth R. Gavis[1*]

1. Department of Molecular Biology, Princeton University, Princeton, New Jersey, 08540
2. Department of Chemical and Biological Engineering, Princeton University, Princeton, New Jersey, 08540
3. Omenn-Darling Bioengineering Institute, Princeton University, Princeton, New Jersey, 08540
4. Department of Chemistry, Princeton University, Princeton, New Jersey, 08540

*correspondence: cmyhrvol@princeton.edu and gavis@princeton.edu

Running title: CRISPR-Cas13 knockdown of *Drosophila* germ granule RNAs

ABSTRACT

Ribonucleoprotein (RNP) germ granules are hallmarks of germ cells across the animal kingdom and are thought to be hubs for post-transcriptional regulation that promote formation of the germ cell precursors. While numerous RNAs are associated with germ granules in *Drosophila*, the functions of many in germline development are poorly understood. Current methods for RNA knockdown, such as RNAi, do not allow local depletion of transcripts such as those found in the germ granules. We leveraged CRISPR-Cas13 to create a subcellular RNA knockdown system and tested it on two mRNAs, *nanos (nos)* and *sarah (sra)*, whose abundance in germ granules differs. Because Cas13 has both *cis* and *trans* cleavage activities, we evaluated the effect of target abundance on off-target RNA depletion. We show on and off-target RNA depletion is coupled when targeting the more abundant *nos* germ granule transcripts. Off-target RNA knockdown is less potent when the system is used for less abundant *sra* transcripts. When *sra* is knocked down in germ granules, we observe defective primordial germ cell migration, and an increase in the calcium indicator GCaMP at the posterior, consistent with *sra* encoding a negative regulator of calcium signaling. In sum, we report an *in vivo* Cas13-based system for subcellular knockdown, evaluate its feasibility, and uncover a novel function for *sra* germ granule transcripts in promoting germline development.

INTRODUCTION

Early in the development of sexually reproducing organisms, cells make a key decision between germline and somatic fates. While the mechanisms and timing that govern this decision vary across organisms, certain features of germline development are conserved. Among these are germ granules, ribonucleoprotein (RNP) granules that are found in germ cells throughout the animal kingdom [1, 2]. Like many types of RNP granules, germ granules are biomolecular condensates composed of RNAs and RNA-binding proteins held together through networks of RNA-RNA, protein-protein, and RNA-protein interactions [3]. As such, they provide compartments for post-transcriptional regulation.

In some animals, including *Drosophila*, germ granules contain maternal determinants necessary for germline formation [1]. In *Drosophila*, the germ granules reside at the posterior pole of the embryo, as components of a maternally derived cytoplasm that is called germ plasm. During embryogenesis, germ granules promote budding of the germline progenitors, called pole cells, from the posterior, and are subsequently incorporated into the pole cells [4]. Within the germ granules, mRNAs are protected from the widespread degradation of other maternal transcripts that occurs during the maternal-zygotic-transition (MZT) [5-7]. Thus, the germ granules provide a supply of maternally-derived mRNAs to the developing pole cells, which are transcriptionally quiescent until gastrulation [8, 9]. These transcripts include *polar granule component* (*pgc*) and *nanos* (*nos*), which have been shown to play roles in pole cell development

including migration to the gonad [10], as well as *Cyclin B* (*Cyc*B). Numerous additional transcripts are likely to associate with the *Drosophila* germ granules based on in situ hybridization studies [11-14], but their roles in promoting germline development remain unknown.

Interrogating the functions of RNAs with complex and dynamic subcellular localizations such as those found in germ granules requires strategies that generate robust subcellular RNA knockdown. Current methods, such as RNA interference (RNAi), are difficult to employ locally in an inducible and temporally regulated manner. Even when expressed under the control of tissue-specific promoters, the RNAi machinery is not readily targeted to specific subcellular regions, limiting its utility for studying transcripts with distinct localizations. Moreover, many mRNAs are enriched rather than exclusively localized to subcellular domains. Indeed, germ granule transcripts are also found at lower concentrations throughout the somatic region of the embryo, where they may play other roles [15-17]. While previous studies have relied on RNAi to investigate the functions of germ granule transcripts, confounding effects on the somatic lineages made it difficult to conclude if the observed defects in germ cell development were due to effects on the germ cells themselves, or were rather influenced by effects on somatic cells that also help promote germline formation [18, 19]. To this end, we leveraged the CRISPR-Cas13 system in an *in vivo* knockdown platform for targeting subcellularly localized RNAs, using *Drosophila* germ granule transcripts as a model (Fig. 1A). Cas13 is an RNA-guided RNA nuclease that can easily be localized to desired subcellular locations, providing a means for local knockdown of target RNAs.

Similar to other CRISPR systems, Cas13 effectors can be co-expressed with CRISPR-RNAs (crRNAs) targeting RNAs of interest for cleavage, making them strong candidates for knockdown applications. Cas13 is activated upon crRNA-target binding, and cleaves the target [20]. Following its activation during these *cis* cleavage events, Cas13 remains active and can cleave other target and non-target molecules in *trans* cleavage events [21, 22]. Cas13d, one of the smallest Cas13 effectors, has been previously used in RNA knockdown applications, with conflicting results. Initial studies using cultured mammalian cells suggested Cas13d can confer highly specific target reduction, with limited off-target effects [23]. In subsequent applications, off-target knockdown was frequent and more severe when Cas13d was used to target highly abundant transcripts of interest or in certain cell types [24-27]. In these studies, the off-target activity was attributed to *trans* cleavage events. This variability has also been observed with Cas13d-mediated knockdown *in vivo*. When the Cas13d machinery was injected into zebrafish and other eukaryotic embryos, strong target RNA knockdown with limited off-target effects was observed using RNA-seq and dual reporter assays, respectively [28]. In *Drosophila*, transgenically expressed Cas13d caused toxicity in flies due to off-target RNA degradation in one knockdown application [29], yet caused no toxicity in another [30]. While *trans* cleavage events were not directly attributed to the off-target activity observed, discrepancies between studies may be explained by Cas13's intrinsic *trans* cleavage activity. These findings highlight the need to monitor potential off-target effects in a Cas13-based knockdown platform in order to

determine what specific applications Cas13d may be most amenable to *in vivo*. For subcellular RNAs, unwanted off-target activity could affect RNAs outside of the subcellular location of interest, as well as other non-target RNAs within the targeted region, adding another layer of complexity (Fig. 1A). As germ granules house many different RNAs, they are an ideal test-case to evaluate the feasibility of a local Cas13d-based RNA knockdown platform.

Here, we applied Cas13d in an RNA knockdown system targeting two germ granule targets: *nos*, which is essential for germline development, and *sarah* (*sra*), a transcript whose function in pole cell formation or development is unknown. As these targets are enriched in germ granules to different extents, we evaluated the effect of target abundance on off-target activity, a factor previously shown to affect *trans* cleavage. Using single molecule fluorescent in situ hybridization (smFISH), we show that on and off-target RNA depletion that is limited to the posterior of the embryo is coupled when we target highly enriched *nos* transcripts. Off-target RNA reduction was less apparent for less abundant *sra* transcripts. Removing *sra* from the germ granules using our strategy led to pole cell migration defects, suggesting a novel role for *sra* in promoting germline development. *sra* encodes a regulator of calcineurin [31] and consistent with this function, Cas13-mediated knockdown of *sra* causes enrichment of the calcium indicator GCaMP prior to pole cell migration. Together, while our results point to using caution when targeting highly abundant transcripts, we show that Cas13d can be used for subcellular knockdown, and we uncover a novel function for germ granule *sra* transcripts in promoting *Drosophila* germline development.

RESULTS

Identifying differentially enriched mRNA targets

To select mRNA targets, we consolidated a list of transcripts that appear to colocalize with germ granules based on previous studies and publicly available in situ hybridization data to select targets from [11, 13, 14, 32]. From these data, 25 transcripts have a distribution characteristic of germ granules (Table S1). From this list, we selected *nos*, whose localization to the germ granules is essential for germline development [33, 34] and *sra*, which encodes a regulator of calcineurin in the calcium signaling pathway [31]. While *sra* has been implicated in *Drosophila* meiosis, ovulation, and plasticity in the neuromuscular junction [31, 35, 36], whether its germ granule localization is functionally significant is unknown, making it an ideal candidate for localized knockdown.

In situ hybridization analysis detected *sra* at the posterior of the early embryo, although it is visibly less enriched than *nos* as compared to the bulk cytoplasm (Fig. S1A). Moreover, *sra* accumulates around budding pole cell nuclei, a distribution characteristic of germ granule mRNAs (Fig. S1B). Using single molecule fluorescence *in situ* hybrization (smFISH), we confirmed that *sra* transcripts are indeed weakly enriched in germ granules in the early embryos,

using *nos* mRNA as a germ granule marker (Fig. 1B). Thus, we conclude that *sra* is a germ granule localized transcript that is less abundant in the germ granules compared to *nos*.

Generating transgenic *Drosophila* strains for Cas13-mediated knockdown

To increase the likelihood of knockdown, we designed CRISPR arrays containing three crRNAs targeting different regions of either *nos* or *sra* transcripts (Fig. S1C-D). Each array was designed such that Cas13d's self-processing activity would produce three individual crRNAs from each array. Transgenic flies expressing each array ubiquitously under the U6 promoter were generated, and the expression of each pre-processed array was confirmed using qPCR (Fig. S1E-F).

We also generated flies for expression of HA-tagged CasFx, a *Drosophila* codon optimized variant of Cas13d, whose cleavage activity was previously demonstrated in flies [32], under Gal4-UAS control. To limit knockdown to the target RNAs within germ granules, we fused CasFx coding sequences to the *nos 3'UTR*. The *nos 3'UTR* serves two purposes: first, it localizes *Cas13* mRNA to germ granules during their assembly, and second, it limits Cas13 protein synthesis to the germ granules beginning in the late stages of oogenesis [32, 37] (Fig. S1G). The resulting *UAS-Cas13-nos3'UTR* transgene was maternally expressed using *mat-tub:Gal4*, and Cas13 protein was detected by anti-HA Western blotting of ovary extracts (Fig. S1H).

On-target and off-target knockdown are coupled for abundant *nos* target transcripts

To investigate knockdown efficiency, we generated flies expressing Cas13 alone or with the *nos* crRNA array, and analyzed the embryos they produced (Fig. 2A). We performed smFISH to detect *nos* in both early embryos expressing the CRISPR-Cas13 machinery targeting *nos* germ granule transcripts ($Cas13^{nos}$) and control embryos expressing Cas13 without crRNAs ($Cas13^{only}$) to compare germ plasm mRNA intensity levels (Fig. 2B and Fig. S2F). Consistently, we observed two populations of embryos, one with reduced mRNA signal intensity and the other with levels comparable to $Cas13^{only}$ control embryos (Fig. 2D and Fig. S2B,H). This bimodal distribution may be explained by mosaic expression of the Gal4 driver used to activate transcription of Cas13 in the ovarian nurse cells, causing variation in the amount of Cas13 protein per embryo [38] (Fig. S2A-A″). Therefore, to evaluate the extent of knockdown (KD), we conservatively defined KD as being outside the lower bound of the confidence interval for the $Cas13^{only}$ control. With this criterion, the difference between +KD and -KD is significant (Fig 2E,H and Fig. S2C).

Due to Cas13's propensity for off-target cleavage events from *trans* cleavage activity, we investigated whether off-target RNA reduction could be detected in $Cas13^{nos}$ embryos. We performed smFISH using probes for another germ granule transcript, either *pgc* or *CycB*, as a Non-Target Control (NTCs) (Fig. 2C and Fig. S2G). Each germ granule NTC exhibited a bimodal distribution that was similar to that of the target *nos* mRNA (Fig 2F and S2D,I).

Consistently, *nos* mRNA fluorescence intensity showed a linear relationship with NTC levels (Fig 2G,I and S2E). As a decrease in NTC levels was only observed when *nos* levels also decreased, these data suggest that off-target RNA reduction is coupled with target reduction. This is consistent with what is expected from Cas13d's *cis* and *trans* cleavage activities in mammalian cells [39].

Late-stage *Cas13^{nos}* embryos have germ cell migration defects

Originating at the posterior of the embryo, the pole cells migrate during gastrulation to populate the gonad [40]. Pole cells lacking *nos* or *pgc* transcripts frequently fail to reach the gonad [41, 42]. Thus, we next asked if Cas13-mediated knockdown of *nos* mRNA and secondary depletion of *pgc* mRNA had effects on pole cell migration. Pole cells were visualized in late-stage embryos during the period of gonad formation using immunohistochemical (IHC) staining for the pole marker, Vasa (Vas) (Fig. 2J). Compared to wild-type embryos, *Cas13^{nos}* embryos exhibited a greater number of pole cells that failed to reach the gonad (Fig. 2K). Notably, the distribution of *Cas13^{nos}* embryos with at least one "lost" pole cell aligns with the bimodal distribution of *nos* and *pgc* mRNA levels in early embryos. In addition to promoting formation of the germline, posterior enrichment of *nos* mRNA is essential for embryonic patterning. Embryos with reduced *nos* at the posterior have fewer than the wild-type 8 abdominal segments [43]. While *Cas13^{nos}* larvae did not exhibit a dramatic loss of abdominal segments, a small number of larvae exhibited segmental fusions (Fig. S2J). Anterior morphology was similar to wild-type in *Cas13^{nos}* larvae. Together, these data suggest that the migration defects observed in *Cas13^{nos}* embryos are likely due to combined effects of *nos* and *pgc* mRNA depletion that is limited to the posterior.

Targeting less enriched *sra* causes reduced off-target knockdown

After we did not observe complete knockdown of *nos*, an abundant germ granule transcript, we next asked if a more complete knockdown of the less enriched *sra* germ granule transcripts could be achieved. We generated transgenic lines expressing an array containing three *sra* crRNAs, and fortuitously isolated one line containing two insertions of the transgene (*sra***). This doubly inserted line expressed more pre-processed *sra* crRNAs than the single insertion (Fig. S1F), which allowed us to test if expressing more crRNAs had an effect on target knockdown.

We performed smFISH for *sra* and *pgc* mRNAs to evaluate mRNA levels in *Cas13^{sra}* and *Cas13^{sra**}* embryos as compared to *Cas13^{only}* embryos (Fig. 3A-C). Given the relatively low amount of localized *sra* mRNA, we calculated an enrichment value for *sra* in the germ plasm at the posterior relative to the cortical cytoplasm. Using this calculation, *Cas13^{sra}* and *Cas13^{sra**}* embryos had significantly less *sra* mRNA germ plasm enrichment compared to *Cas13^{only}* embryos (Fig. 3D). Moreover, many of these embryos had enrichment values around 0, which suggests that almost complete knockdown of a low abundance target is more achievable even with a single crRNA insertion.

Reduced NTC reduction for a less abundant target

In previous studies, non-target RNA reduction from *trans* cleavage events in cultured cells was less severe when Cas13d was used to target low abundance transcripts [24-26, 39]. To determine if this was also true in our system, we calculated *pgc* enrichment, and found there was no significant difference in *pgc* enrichment between $Cas13^{only}$, $Cas13^{sra}$, and $Cas13^{sra**}$ (Fig. 3E). Furthermore, there was not a linear relationship between *sra* and *pgc* enrichment in $Cas13^{sra}$ and $Cas13^{sra**}$ embryos, though reduced *pgc* enrichment was only observed when reduced *sra* enrichment was also observed (Fig. 3F,G). Slight variations in *pgc* enrichment occur even in wild-type embryos (Fig. 3H). Together, these data indicate that indeed, the effects of NTC knockdown are less pronounced for Cas13-mediated knockdown against a low abundance target.

We wondered if the observed reduction in off-target effects in $Cas13^{sra}$ and $Cas13^{sra**}$ affects other germ plasm mRNAs. We performed smFISH in $Cas13^{nos}$, $Cas13^{sra}$, and $Cas13^{sra**}$ embryos, and probed for *nos*. Unlike the bimodal distribution of *nos* levels observed in $Cas13^{nos}$, *nos* germ plasm levels were not significantly different in $Cas13^{sra}$ and $Cas13^{sra**}$ embryos (Fig. 3I). Moreover, even the lowest *nos* level in $Cas13^{sra}$ and $Cas13^{sra**}$ embryos was higher than those of $Cas13^{nos}$ embryos exhibiting knockdown, suggesting that off-target cleavage events alone are not sufficient to produce knockdown comparable to that achieved with a crRNA for a specific target. Together, these data indicate that our Cas13d-based system confers more specific subcellular knockdown against a lower abundance target.

sra promotes pole cell migration

The ability to deplete *sra* mRNAs more completely without obvious off-target effects allowed us to investigate a role for *sra* in pole cells. As a previous study found that the *sra 3'UTR* confers a translational onset prior to pole cell migration [32], we asked if Cas13-mediated knockdown of *sra* transcripts might lead to abnormal pole cell migration. Anti-Vas IHC showed an increased frequency of pole cell migration defects in both $Cas13^{sra}$ and $Cas13^{sra**}$ embryos (Fig. 4A-B and S3). Over 10% of $Cas13^{sra}$ and $Cas13^{sra**}$ embryos had more than four "lost" pole cells, with some located far from the gonads (Fig. 4B) – a more severe effect compared to that of $Cas13^{nos}$ embryos. These data are in agreement with evidence for more frequent complete knockdown of *sra* (Fig. 3). *sra* encodes calcipressin, a negative regulator of calcineurin [31, 44-47]. We therefore investigated whether Cas13-mediated knockdown of *sra* affects calcium waves occurring in the embryo prior to pole cell migration, using the calcium sensor GCaMP [48] expressed transgenically in the germline (Fig. 4C). Genetic limitations prevented us from introducing a pole cell marker into flies expressing the Cas13 machinery together with GCaMP. Instead, we visualized at GCaMP enrichment at the posterior in embryos where pole cells were morphologically visible. sra^{Cas13} embryos exhibited a small but significant increase in GCaMP enrichment in the pole cells at the posterior prior to migration (Fig. 4D). Together, these data suggest that *sra* germ granule mRNAs may promote pole cell migration during embryogenesis through the calcium signaling pathway.

DISCUSSION

While germ granules are a common feature of germline development across species, the roles of many germ granule mRNAs have yet to be interrogated due to a lack of methods for probing the functions of subcellularly enriched transcripts. Here, we implement a Cas13d-based RNA knockdown platform to investigate those functions in *Drosophila*. Using this system, we begin to study the feasibility of this strategy and uncover a novel function for one germ granule transcript, *sra*.

Cas13-based subcellular RNA knockdown

To study complex questions about RNA regulation *in vivo*, the ability to manipulate the expression of individual components is essential for a subcellular mRNA knockdown system. We achieved subcellular RNA knockdown of germ granule enriched mRNAs by targeting Cas13 protein production to *Drosophila* germ granules using the *nos* 3′UTR, while ubiquitously expressing crRNAs. As Cas13 proteins are exogenous to eukaryotic systems, achieving local knockdown using localization tags at the transcript and/or protein level is promising. In addition to localization, temporal control may also be imposed to study particular time periods. We used the *nos* 3′UTR to initiate Cas13 protein synthesis during the late stages of oogenesis. For our specific application, 3′UTRs of other germ granule RNAs known to initiate translation only in the embryo [32] may be used to probe temporal requirements for these RNAs. Ubiquitously expressing crRNAs, as in our strategy, adds additional flexibility. Previously generated crRNA-expressing animals may be crossed to various localized-Cas13-expressing animals, to deplete the same transcripts in different subcellular domains. The potential adaptability of a Cas13-based RNA knockdown system makes it a strong fit for investigating roles for localized RNAs in regulating developmental decisions.

Along with flexibility, limited off-target activity is an essential component of any knockdown system. Given Cas13's propensity for *trans* cleavage activity, we measured target and NTC mRNA depletion on a per embryo basis using smFISH analysis. Indeed, we observed off-target activity when targeting *nos* mRNA. While we cannot directly attribute this off-target activity to *trans* cleavage events occurring *in vivo,* the correlation between target and NTC knockdown has also been observed for Cas13d in mammalian cell culture [39]. As target abundance has previously been shown to affect Cas13's propensity for *trans* cleavage [24-27], we took advantage of *sra*'s weak enrichment at the posterior to evaluate NTC depletion when targeting a less abundant RNA. Indeed, targeting *sra* for knockdown caused more robust on-target depletion together with less off-target effects. Cas13d's varying propensity for *trans* cleavage activity depending on target abundance may provide one explanation for confounding results in previous *in vivo* applications, which target different RNAs in different cell contexts [28, 30, 49]. Based on our data, we conclude that Cas13d may be better suited for studying low abundance targets *in vivo*. Our results also suggest that *cis* and *trans* cleavage activities can still

be coupled when Cas13 is transgenically expressed *in vivo*, which could potentially be useful for applications which require robust local depletion of many different RNA targets at once.

In future applications, *trans* cleavage may be limited using different Cas13 effectors shown to have less *trans* cleavage activity in cell contexts such as Cas13b [24] or high-fidelity Cas13 variants [27], which are engineered to still have robust *cis* cleavage with the absence of *trans* cleavage. Despite limitations due to off-target activity, Cas13d-based RNA knockdown resulted in robust reduction of a less enriched germ granule mRNA, *sra*, which allowed us to begin interrogating its function in the context of germ cell development.

Interrogating germ granule mRNAs and *sra* function

Although numerous mRNAs are thought to occupy *Drosophila* germ granules [10–13,49], only a small subset have been functionally characterized. As germ granules supply maternally deposited transcripts to the mostly transcriptionally quiescent pole cells [8, 9], it seems likely that other germ granules outside of the subset also play roles in promoting germline development. Our finding that Cas13-mediated knockdown of *sra* results in defective pole cell migration supports this idea. As *sra* negatively regulates calcineurin activity [44-47], one potential mechanism for germ granule localized *sra* mRNA to promote germ cell migration is by modulation of calcium signaling. While we have not been able to directly test the effect of *sra* knockdown in migrating pole cells, our finding that Cas13-mediated *sra* knockdown leads to elevated GCaMP in the pre-migratory pole cells supports this hypothesis. Modulation of calcium signaling has been previously observed to promote cell migration processes [50, 51] and effects on calcium signaling are also well documented in tumor cell migration [52-54]. Polarization of calcium waves promotes convergent extension in amphibians during gastrulation [55-57]. Thus, modulation of calcium fluxes in pole cells by Sra protein may be one developmental consequence of germ granule mRNA localization.

ACKNOWLEDGEMENTS

We are grateful to M. Wolfner for the *UASp-GCaMP* flies and T. Schüpbach for the Anti-Vas antibody. We thank G. Laevsky and S. Wang in the Princeton Confocal imaging facility, a Nikon center for excellence in the Department of Molecular Biology, for assistance with microscopy, S. Chatterjee for cloning the *UAS-Cas13-nos3′UTR* plasmid, K.Y. Lee for generating the *nos* riboprobe used in Fig. S1, and A. Hakes and M. Kilwein for technical advice.

METHODS

Drosophila strains and genetics

The following fly stocks were obtained: *UASp-GCaMP* (gift from M. Wolfner [48]), *maternal-tubulin:Gal4*^{v37} (BDSC #7063). For Cas13-mediated knockdown, flies homozygous for both the *maternal-tubulin:Gal4*^{v37}driver on chromosome 2 and a crRNA array on chromosome 3 were crossed to flies homozygous for the *UAS-Cas13-nos3'UTR* transgene (see below). *Cas13*^{only} control flies were generated by crossing flies homozygous for the *mat-tub:Gal4* driver to flies homozygous for the *UAS-Cas13-nos3'UTR* transgene.

crRNA design

crRNAs were designed to target the most representative isoforms of each target in the 0-2 hour embryo, based on FLYBase high throughput expression data. *nos-RA* (FLYBase ID:FBtr0083732) and *sra-RA* (FLYBase ID: FBtr0083255) were chosen as targets.

Taking advantage of Cas13's crRNA processing activity, three unique Cas13d crRNAs were designed per target and expressed as an array. Each guide region was designed using the publicly available Cas13design tool [58, 59]. To generate guide RNAs, *Drosophila* was selected as the model organism, and the associated FlyBASE ID for each target isoform was inputted. Three sequences complementary to unique regions within each target transcript were selected. All guide sequences are shown in Table S2. All predicted guides had scores of above 85%, and regions targeted coding sequences (CDS) were selected over untranslated regions (UTRs) when possible. For compatibility with Cas13d, the direct repeat sequence (Table S2) was added at the 5' end, followed by a guide sequence to create a complete crRNA. For each target, the three crRNAs were synthesized as an array followed by a terminator sequence (Table S2) with flanking NotI and PstI digest sites (Genewiz).

Drosophila transgene generation

crRNA arrays were cloned into a vector previously used to express Cas13d crRNAs in *Drosophila* [49]. The *nos* crRNA array was digested using NotI and the blunt cutter MslI. The vector was digested using NotI and PstI digest sites and end-filled using T4 polymerase, prior to ligating the *nos* crRNA insert into the vector. The *sra* crRNA array was digested using NotI and PstI digest sites, and ligated into NotI and PstI digested vector. crRNA arrays were was inserted at the attP40 site on the second chromosome using the ΦC31 recombinase system.

To generate the *UAS-Cas13-nos3'UTR* transgene, the *Drosophila* codon optimized Cas13d sequence (CasFX4; [30]) was synthesized, including 3xHA tag just before the first CasFX4 codon (Genewiz), flanked by KpnI and HindIII sites. This sequence was inserted together with a HindIII-NotI fragment containing the *nos* 3′UTR and 75 bp of 3′ genomic DNA between KpnI and NotI sites of pattB-UASp from which the K10 3′UTR sequences were removed. The *UAS-Cas13-nos3'UTR* transgene was inserted at the VK0033 site on the third chromosome using the ΦC31 recombinase system.

In situ hybridization

For immunohistochemical *in situ* hybridization, embryos were collected for 2.5 hours at 25 °C. Embryos were dechorinated, fixed, and devitellinized using methanol as previously described [60], and stored in methanol at -20 °C for up to two weeks. In situ hybridization was performed as previously described with using digoxigenin-labeled riboprobes [37]. For the *sra* riboprobe, cDNA (#LD15403) from the *Drosophila Genomics Resource Center* was used as a template.

For smFISH, embryos were collected on yeasted apple juice plates for 2.5 hours at 25 °C and staged by nuclear density and morphological features for nuclear cycle 0. Embryos were dechorinated, fixed, hand peeled as previously described [60], dehydrated stepwise into methanol and stored at -20 °C for up to one week. smFISH was performed as previously described [60] after rehydrating embryos stepwise into PBST (PBS/0.1% Tween20), and the samples were then mounted in Vectashield. Prior to imaging, embryos were stored overnight at 4°C with the coverslip facedown. For *sra* RNAs, a custom *sra*-570 probe set was generated (Stellaris).

Confocal microscopy and quantification of smFISH

Confocal microscopy was performed using a Nikon A1 scanning confocal microscope using GaAsp detectors and a 60 × 1.4 NA oil immersion objective, with the exception of Figure S2A, where a 40 x 1.3 NA oil immersion objective was used. Z-series were captured using a 1.5 µm step-size. Within each experiment, imaging parameters among samples were kept identical. smFISH was quantified by generating “summed slice intensity” projections in FIJI. Fluorescence intensities in Fig. 2 and S2 were calculated by measuring the integrated density of the germ plasm and of a "background" region of the same area outside of the embryo, and subtracting these two values. Enrichments in Fig. 3 were calculated by measuring the integrated density of the germ plasm within an ROI selected using the germ plasm marker. The ROI was moved to a region of the cortical cytoplasm to measure a background value, which was then subtracted from the germ plasm value.

Immunohistochemistry

Embryos were collected on yeasted apple juice plates for six hours at 25 °C, then aged for 20 hours at 18°C. Anti-Vas IHC was performed as previously described [61] to detect pole cells in Bownes staged 14-15 embryos with the following antibodies: 1:500 rabbit anti-phospho-Vas (gift of T. Schüpbach) and 1:500 biotin goat anti-rabbit (Jackson Immuno Research Laboratories). Embryos were mounted in 80% glycerol and pole cells were visualized and counted on a Zeiss compound microscope. Images of representative embryos were captured using a Nikon DsQi-2 microscope, with a 20 X 0.75 NA air objective and DIC optics.

Larval cuticle preparation

Embryos were collected on yeasted apple juice plates at room temperature over one day, aged for one day, and stored at 4 °C for up to one week. Cuticle preparations were performed as

previously described [62], mounted in Hoyer's media, and segments were counted on a Zeiss compound microscope.

Live-imaging and quantification of GCaMP

For live-imaging, approximately 2.5 hour old embryos were collected on yeasted apple juice plates at 25 °C, dechorinated, placed onto a #1.5 coverslip using a paintbrush, and covered in a drop of Halocarbon 200 Oil. Live-imaging was performed on a Nikon A1 scanning confocal microscope using GaAsp detectors and a 40 x 1.3 NA oil objective, which was focused to the middle of the embryo, and images were captured every forty seconds. For GCaMP fluorescence quantification, a single frame from each video was selected where the pole cells were in a similar plane. Integrated density was measured for the germ plasm, as well as for a region of the cortical cytoplasm of the same area. Enrichment was calculated by subtracting the germ plasm integrated density from the cortical cytoplasm integrated density.

RT-qPCR

Ovaries were dissected from wild-type female or females homozygous for either crRNA transgene and flash frozen. RNA was extracted from 20 ovaries per sample using the *Quick*-RNA™ Miniprep Plus Kit (Zymo Research). Genomic DNA removal and cDNA generation were performed using the Quantitect Reverse Transcription Kit. In place of RT primer mix, transgene specific primers (Table S3) designed for each crRNA were used to generate cDNAs. qPCR was performed using SYBR Green PCR Master Mix (Thermo Fisher Scientific) and the StepOnePlus Real-Time PCR system (Applied Biosystems) according to manufacturer's instructions using the same gene specific primers. Three technical replicates were performed per sample. For analysis, technical replicates were averaged, and the mean CT was used to calculate the relative gene expression per sample normalized to the wild-type control by the ΔΔCT method [63], with *rp49* used as the reference gene.

Immunoblotting

Flash frozen ovaries from either of two independent transgenic *Cas13-nos3'UTR* lines or with the *mat-tub:GAL4* driver alone were thawed and dissolved in 5 µl of sample buffer (0.125 M Tris-HCl (pH 6.8), 4% SDS, 20% glycerol, 5 M urea, 0.01% bromophenol blue, and 0.1 M DTT) per ovary and boiled for 4 minutes. The samples were run on a 9% SDS-PAGE gel, and immunoblotting was performed as previously described [63] using the following antibodies: 1:1000 rabbit anti-HA (Cell Signaling Technologies #C29F4) and 1:2000 HRP donkey anti-rabbit (GE Healthcare). The blot was imaged using an iBright FL1000 imaging system. Due to an interaction between the HA and tubulin antibodies, the same blot was stripped using Restore Western Blot Stripping Buffer (Thermo Scientific), reprobed with the following antibodies: 1:5000 mouse ascites (Sigma) and 1:1000 HRP sheep anti-mouse (NA931), and reimaged.

Figure 1

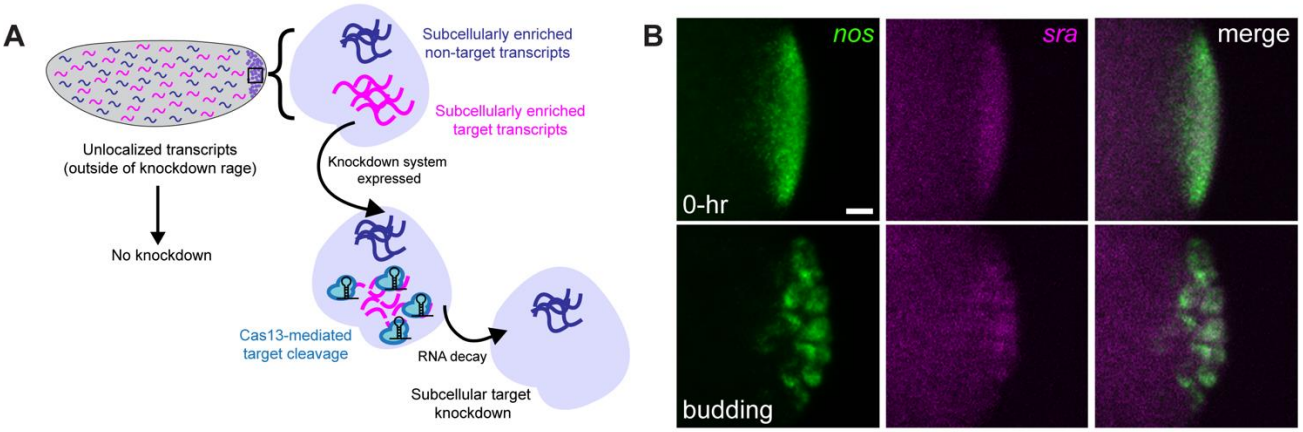

Figure 1: A Cas13-based method for localized RNA knockdown. (A) Strategy for Cas13-mediated knockdown of germ granule transcripts. Spatial control over degradation of a target mRNA (magenta) is conferred by localizing Cas13 protein synthesis to germ granules. (B) Summed slice intensity projections of *nos* (green) and *sra* (magenta) mRNAs detected by smFISH in 0 hour old and pole-bud stage embryos. *sra* and *nos* are colocalized in germ granules through pole cell formation, with *sra* less enriched than *nos*. Scale bar = 10 µm.

Figure 2

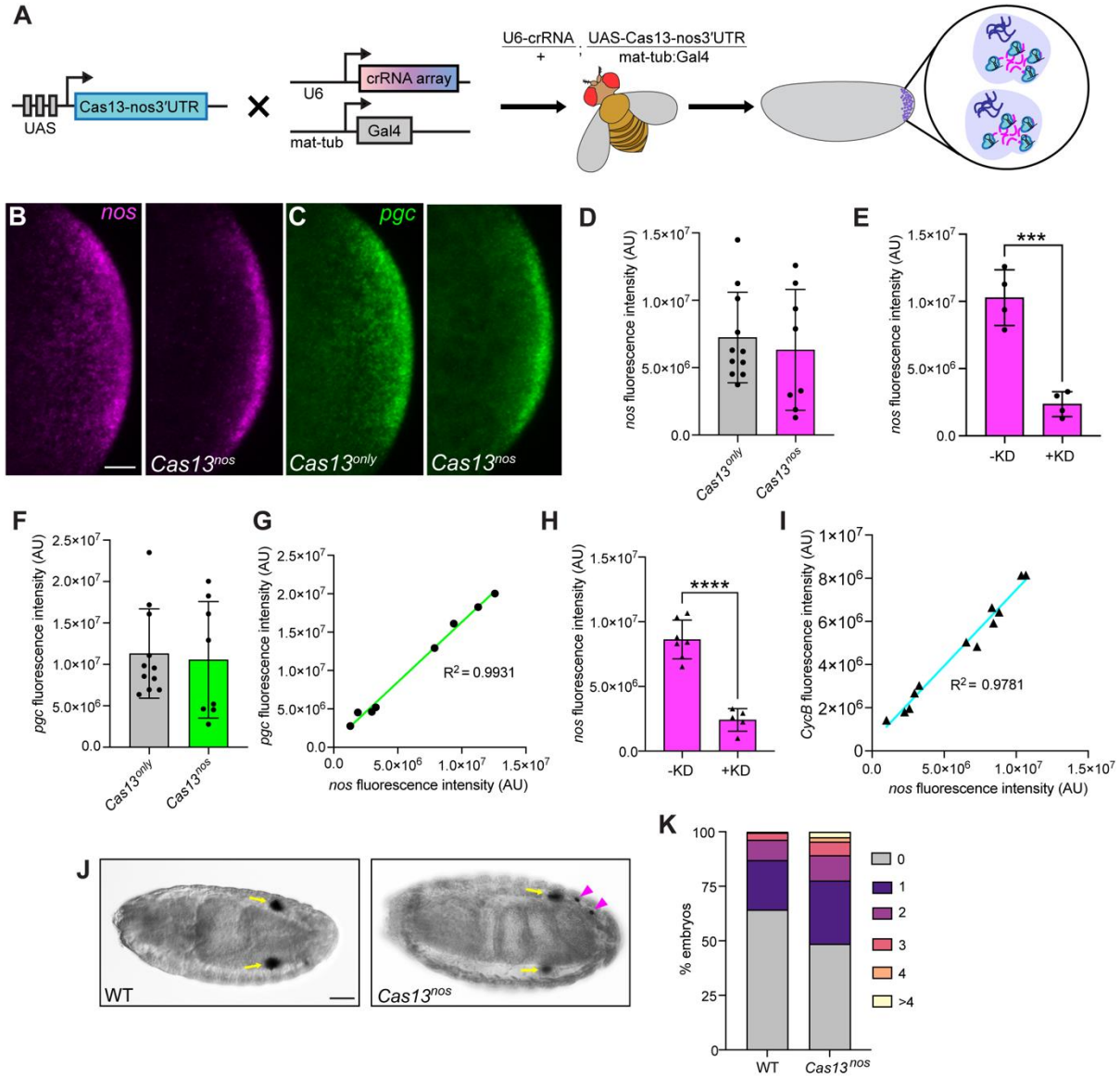

Figure 2: On and off-target activity are coupled in *Cas13^{nos}* embryos. (A) Scheme to produce females co-expressing Cas13 and crRNAs. Cas13-mediated knockdown occurs in eggs produced by these females. (B, C) Summed slice intensity projections of early *Cas13^{only}* and *Cas13^{nos}* embryos, with *nos* (magenta, B) and *pgc* (green, C) detected by smFISH. (D) Quantification of *nos* fluorescence intensity in germ granules for embryos from a single experiment (n = 11 embryos for *Cas13^{only}*, n = 8 embryos for *Cas13^{nos}*). (E) Comparison of *nos* fluorescent intensities between *Cas13^{nos}* embryos where knockdown occurred and embryos without knockdown based on the bimodally distributed data points. (F) Quantification of *pgc* fluorescence intensity in germ granules from the same embryos as in (E). (G) Simple linear regression analysis of the *nos* and *pgc* levels for individual embryos (R^2 = 0.9931, y = 1.562x + 686498). (H) Comparison of *nos* fluorescence intensities between *Cas13^{nos}* embryos with and without knockdown from a second experimental replicate (n = 12 embryos). (I) Simple linear

regression analysis of the *nos* and *CycB* levels for individual embryos (R^2 = 0.9781, y = 0.7040x + 418194). (J) DIC images of Bownes stage fourteen *Cas13*^{only} and *Cas13*^{nos} embryos. Anti-Vas immunohistochemistry was used to detect pole cells. Pole cells populating the gonad are indicated with yellow arrows, "lost" pole cells with magenta arrowheads. (K) Quantification of embryos with the indicated number of lost post cells (n = 459 embryos for *Cas13*^{only}, n = 658 embryos for *Cas13*^{nos}). Data points represent individual embryos. Unpaired t-test was used in E and H, ****p<0.0001 and ***p<0.001. Scale bars = 10 µm (B, C) and 50 µm (J, J').

Figure 3

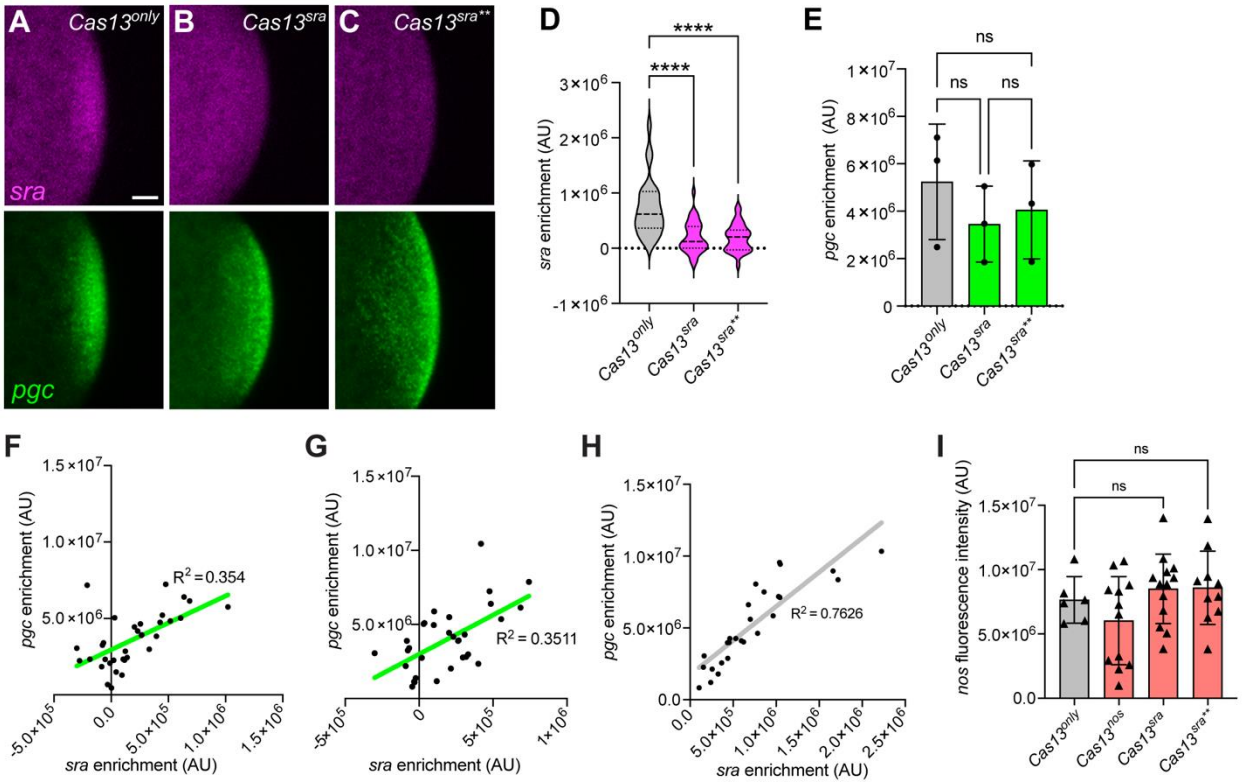

Figure 3: Cas13-mediated knockdown of a lower abundance target is more effective, with less off-target activity. (A-C) Summed slice intensity projections of early *Cas13*^{only} (A), *Cas13*^{sra} (B) and *Cas13*^{sra**} (C) embryos with *sra* (magenta) and *pgc* (green) detected by smFISH. (D) Violin plot of *sra* enrichment in germ granules for three experimental replicates (n = 27 embryos for *Cas13*^{only}, n = 35 embryos for *Cas13*^{sra}, and n = 32 embryos for *Cas13*^{sra**}). (E) Quantification of mean *pgc* enrichment for the three experimental replicates. (F-H) Simple linear regression of the *sra* and *pgc* enrichment for *Cas13*^{sra} (F; R^2=0.3540, y = 3.516x + 2955538), *Cas13*^{sra**} (G; R^2 = 0.3511, y = 5.278x + 2994481), and *Cas13*^{only} (H; R^2= 0.7626, y = 4.759x + 1743067) embryos. Linear regression of *Cas13*^{only} shows scatter of *pgc* enrichment intensity in control scenario. (I) Quantification of *nos* fluorescence intensity for the indicated genotypes. Data from the experiment in Fig. 2 H-I and Fig. S2 H-I for *Cas13*^{only} and *Cas13*^{nos} embryos are included alongside data from *Cas13*^{sra} and *Cas13*^{sra**}embryos, which were all collected at the same time to perform *nos* smFISH. Data points represent individual embryos in all graphs except for the means shown in E. Ordinary one-way and multiple comparisons ANOVA were performed in D, E, and I, ****p<0.0001, ns = not significant. Scale bar = 10 µm.

Figure 4

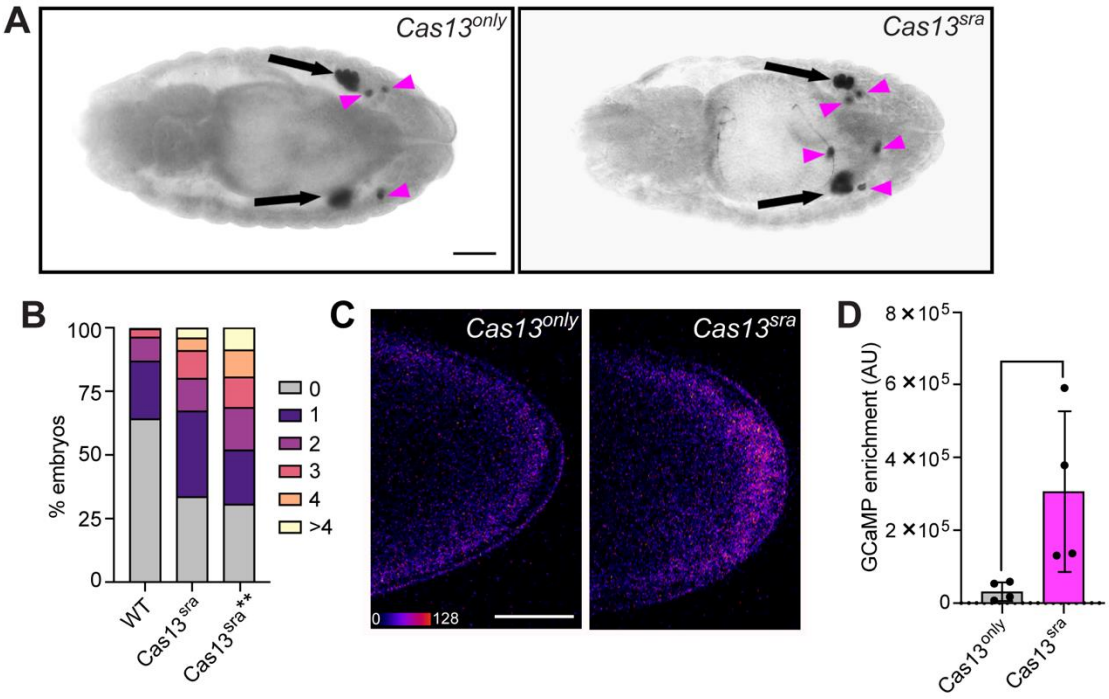

Figure 4: *sra* promotes pole cell migration. (A) DIC images of *Cas13*^{sra} and *Cas13*^{sra**} Bownes stage 14 embryos. Pole cells were detected with anti-Vas immunohistochemistry. Black arrows indicate pole cells in gonads, and magenta arrowheads indicate "lost" pole cells. (C) Quantification of embryos with the indicated number of lost pole cells (n = 101 embryos for *Cas13*^{sra} and n = 150 embryos for *Cas13*^{sra**}). (D) Still images from time-lapse imaging of the GCaMP sensor in *Cas13*^{only} and *Cas13*^{sra} embryos. Single sections through the middle of the embryo are shown. (E) Quantification of GCaMP fluorescence intensity (n = 4 embryos for each genotype). Data points represent individual embryos. Unpaired t-test was used in E, *p<0.05. Scale bar = 50 µm (B), and 100 µm for GCaMP images.

REFERENCES

1. Strome S, Updike D. Specifying and protecting germ cell fate. Nat Rev Mol Cell Biol. 2015;16(7):406-16. Epub 2015/07/01. doi: 10.1038/nrm4009. PubMed PMID: 26122616; PubMed Central PMCID: PMCPMC4698964.

2. Cassani M, Seydoux G. P-body-like condensates in the germline. Semin Cell Dev Biol. 2023. Epub 20230703. doi: 10.1016/j.semcdb.2023.06.010. PubMed PMID: 37407370.

3. Putnam A, Thomas L, Seydoux G. RNA granules: functional compartments or incidental condensates? Genes Dev. 2023;37(9-10):354-76. Epub 20230503. doi: 10.1101/gad.350518.123. PubMed PMID: 37137715; PubMed Central PMCID: PMCPMC10270194.

4. Mahowald AP. Assembly of the *Drosophila* germ plasm. Int Rev Cytol. 2001;203:187-213.

5. Schulz KN, Harrison MM. Mechanisms regulating zygotic genome activation. Nat Rev Genet. 2019;20(4):221-34. doi: 10.1038/s41576-018-0087-x. PubMed PMID: 30573849; PubMed Central PMCID: PMCPMC6558659.

6. Tadros W, Lipshitz HD. The maternal-to-zygotic transition: a play in two acts. Development. 2009;136(18):3033-42. doi: 10.1242/dev.033183. PubMed PMID: 19700615.

7. Siddiqui NU, Li X, Luo H, Karaiskakis A, Hou H, Kislinger T, et al. Genome-wide analysis of the maternal-to-zygotic transition in *Drosophila* primordial germ cells. Genome Biol. 2012;13(2):R11. doi: 10.1186/gb-2012-13-2-r11. PubMed PMID: 22348290; PubMed Central PMCID: PMC3334568.

8. Su TT, Campbell SD, O'Farrell PH. The cell cycle program in germ cells of the *Drosophila* embryo. Dev Biol. 1998;196(2):160-70. Epub 1998/05/13. doi: 10.1006/dbio.1998.8855. PubMed PMID: 9576829.

9. Van Doren M, Williamson AL, Lehmann R. Regulation of zygotic gene expression in *Drosophila* primordial germ cells. Curr Biol. 1998;8(4):243-6. PubMed PMID: 9501989.

10. Trcek T, Lehmann R. Germ granules in Drosophila. Traffic. 2019;20(9):650-60. Epub 2019/06/21. doi: 10.1111/tra.12674. PubMed PMID: 31218815; PubMed Central PMCID: PMCPMC6771631.

11. Lecuyer E, Yoshida H, Parthasarathy N, Alm C, Babak T, Cerovina T, et al. Global analysis of mRNA localization reveals a prominent role in organizing cellular architecture and function. Cell. 2007;131(1):174-87. Epub 2007/10/10. doi: 10.1016/j.cell.2007.08.003. PubMed PMID: 17923096.

12. Wilk R, Hu J, Blotsky D, Krause HM. Diverse and pervasive subcellular distributions for both coding and long noncoding RNAs. Genes Dev. 2016;30(5):594-609. Epub 2016/03/06. doi: 10.1101/gad.276931.115. PubMed PMID: 26944682; PubMed Central PMCID: PMCPMC4782052.

13. Tomancak P, Beaton A, Weiszmann R, Kwan E, Shu S, Lewis SE, et al. Systematic determination of patterns of gene expression during *Drosophila* embryogenesis. Genome Biol. 2002;3(12):RESEARCH0088. PubMed PMID: 12537577; PubMed Central PMCID: PMC151190.

14. Tomancak P, Berman BP, Beaton A, Weiszmann R, Kwan E, Hartenstein V, et al. Global analysis of patterns of gene expression during Drosophila embryogenesis. Genome Biol. 2007;8(7):R145. doi: 10.1186/gb-2007-8-7-r145. PubMed PMID: 17645804; PubMed Central PMCID: PMC2323238.

15. Bergsten SE, Gavis ER. Role for mRNA localization in translational activation but not spatial restriction of *nanos* RNA. Development. 1999;126:659-69.

16. Little SC, Sinsimer KS, Lee JJ, Wieschaus EF, Gavis ER. Independent and coordinate trafficking of single *Drosophila* germ plasm mRNAs. Nat Cell Biol. 2015;17(5):558-68. doi: 10.1038/ncb3143. PubMed PMID: 25848747.

17. Trcek T, Douglas TE, Grosch M, Yin Y, Eagle WVI, Gavis ER, et al. Sequence-independent self-assembly of germ granule mRNAs into homotypic clusters. Mol Cell. 2020;78(5):941-50.e12. Epub 20200527. doi: 10.1016/j.molcel.2020.05.008. PubMed PMID: 32464092; PubMed Central PMCID: PMCPMC7325742.

18. Jankovics F, Henn L, Bujna A, Vilmos P, Spirohn K, Boutros M, et al. Functional analysis of the *Drosophila* embryonic germ cell transcriptome by RNA interference. PLoS One. 2014;9(6):e98579. Epub 2014/06/05. doi: 10.1371/journal.pone.0098579. PubMed PMID: 24896584; PubMed Central PMCID: PMCPMC4045815.

19. Liu N, Lasko P. Analysis of RNA interference lines Identifies new functions of maternally-expressed genes involved in embryonic patterning in *Drosophila melanogaste*r. G3 (Bethesda). 2015;5(6):1025-34. Epub 2015/04/04. doi: 10.1534/g3.115.017517. PubMed PMID: 25834215; PubMed Central PMCID: PMCPMC4478533.

20. Abudayyeh OO, Gootenberg JS, Konermann S, Joung J, Slaymaker IM, Cox DB, et al. C2c2 is a single-component programmable RNA-guided RNA-targeting CRISPR effector. Science. 2016;353(6299):aaf5573. Epub 20160602. doi: 10.1126/science.aaf5573. PubMed PMID: 27256883; PubMed Central PMCID: PMCPMC5127784.

21. East-Seletsky A, O'Connell MR, Knight SC, Burstein D, Cate JH, Tjian R, et al. Two distinct RNase activities of CRISPR-C2c2 enable guide-RNA processing and RNA detection.

Nature. 2016;538(7624):270-3. Epub 20160926. doi: 10.1038/nature19802. PubMed PMID: 27669025; PubMed Central PMCID: PMCPMC5576363.

22. Liu L, Li X, Wang J, Wang M, Chen P, Yin M, et al. Two distant catalytic sites are responsible for C2c2 RNase activities. Cell. 2017;168(1-2):121-34 e12. Epub 20170112. doi: 10.1016/j.cell.2016.12.031. PubMed PMID: 28086085.

23. Konermann S, Lotfy P, Brideau NJ, Oki J, Shokhirev MN, Hsu PD. Transcriptome engineering with RNA-targeting Type VI-D CRISPR effectors. Cell. 2018;173(3):665-76 e14. Epub 20180315. doi: 10.1016/j.cell.2018.02.033. PubMed PMID: 29551272; PubMed Central PMCID: PMCPMC5910255.

24. Ai Y, Liang D, Wilusz JE. CRISPR/Cas13 effectors have differing extents of off-target effects that limit their utility in eukaryotic cells. Nucleic Acids Res. 2022;50(11):e65. doi: 10.1093/nar/gkac159. PubMed PMID: 35244715; PubMed Central PMCID: PMCPMC9226543.

25. Kelley CP, Haerle MC, Wang ET. Negative autoregulation mitigates collateral RNase activity of repeat-targeting CRISPR-Cas13d in mammalian cells. Cell Rep. 2022;40(7):111226. doi: 10.1016/j.celrep.2022.111226. PubMed PMID: 35977479; PubMed Central PMCID: PMCPMC9809062.

26. Shi P, Murphy MR, Aparicio AO, Kesner JS, Fang Z, Chen Z, et al. Collateral activity of the CRISPR/RfxCas13d system in human cells. Commun Biol. 2023;6(1):334. Epub 20230328. doi: 10.1038/s42003-023-04708-2. PubMed PMID: 36977923; PubMed Central PMCID: PMCPMC10049998.

27. Tong H, Huang J, Xiao Q, He B, Dong X, Liu Y, et al. High-fidelity Cas13 variants for targeted RNA degradation with minimal collateral effects. Nat Biotechnol. 2023;41(1):108-19. Epub 20220811. doi: 10.1038/s41587-022-01419-7. PubMed PMID: 35953673.

28. Kushawah G, Hernandez-Huertas L, Abugattas-Nunez Del Prado J, Martinez-Morales JR, DeVore ML, Hassan H, et al. CRISPR-Cas13d induces efficient mRNA knockdown in animal embryos. Dev Cell. 2020;54(6):805-17 e7. Epub 20200807. doi: 10.1016/j.devcel.2020.07.013. PubMed PMID: 32768421.

29. Buchman AB, Brogan DJ, Sun R, Yang T, Hsu PD, Akbari OS. Programmable RNA targetingusing CasRx in flies. CRISPR J. 2020;3(3):164-76. doi: 10.1089/crispr.2020.0018. PubMed PMID: 32584145; PubMed Central PMCID: PMCPMC7307691.

30. Huynh N, Depner N, Larson R, King-Jones K. A versatile toolkit for CRISPR-Cas13-based RNA manipulation in *Drosophila*. Genome Biol. 2020;21(1):279. Epub 2020/11/19. doi: 10.1186/s13059-020-02193-y. PubMed PMID: 33203452; PubMed Central PMCID: PMCPMC7670108.

31. Takeo S, Tsuda M, Akahori S, Matsuo T, Aigaki T. The calcineurin regulator Sra plays an essential role in female meiosis in *Drosophila*. Curr Biol. 2006;16(14):1435-40. Epub 2006/07/25. doi: S0960-9822(06)01677-0 [pii] 10.1016/j.cub.2006.05.058. PubMed PMID: 16860743.

32. Rangan P, DeGennaro M, Jaime-Bustamante K, Coux RX, Martinho RG, Lehmann R. Temporal and spatial control of germ-plasm RNAs. Curr Biol. 2009;19(1):72-7. Epub 2008/12/27. doi: 10.1016/j.cub.2008.11.066. PubMed PMID: 19110432; PubMed Central PMCID: PMCPMC2766415.

33. Kobayashi S, Yamada M, Asaoka M, Kitamura T. Essential role of the posterior morphogen *nanos* for germline development in *Drosophila*. Nature. 1996;380:708-11.

34. Gavis ER, Chatterjee S, Ford NR, Wolff LJ. Dispensability of *nanos* mRNA localization for abdominal patterning but not for germ cell development. Mech Dev. 2008;125:81-90.

35. Ejima A, Tsuda M, Takeo S, Ishii K, Matsuo T, Aigaki T. Expression level of *sarah*, a homolog of DSCR1, is critical for ovulation and female courtship behavior in *Drosophila melanogaster*. Genetics. 2004;168(4):2077-87. doi: 10.1534/genetics.104.029934. PubMed PMID: 15611177; PubMed Central PMCID: PMCPMC1448750.

36. Armstrong NS, Frank CA. The calcineurin regulator Sarah enables distinct forms of homeostatic plasticity at the *Drosophila* neuromuscular junction. Front Synaptic Neurosci. 2022;14:1033743. Epub 20230104. doi: 10.3389/fnsyn.2022.1033743. PubMed PMID: 36685082; PubMed Central PMCID: PMCPMC9846150.

37. Gavis ER, Lehmann R. Localization of *nano*s RNA controls embryonic polarity. Cell. 1992;71:301-13.

38. Rorth P. Gal4 in the *Drosophila* female germline. Mech Dev. 1998;78:113-8.

39. Hart SK, Wessels HH, Mendez-Mancilla A, Muller S, Drabavicius G, Choi O, et al. Low copy CRISPR-Cas13d mitigates collateral RNA cleavage. bioRxiv. 2024. Epub 20240514. doi: 10.1101/2024.05.13.594039. PubMed PMID: 38798586; PubMed Central PMCID: PMCPMC11118291.

40. Richardson BE, Lehmann R. Mechanisms guiding primordial germ cell migration: strategies from different organisms. Nat Rev Mol Cell Biol. 2010;11(1):37-49. doi: 10.1038/nrm2815. PubMed PMID: 20027186; PubMed Central PMCID: PMCPMC4521894.

41. Asaoka M, Sano H, Obara Y, Kobayashi S. Maternal Nanos regulates zygotic gene expression in germline progenitors of *Drosophila melanogaster*. Mech Dev. 1998;78(1-2):153-8.

42. Nakamura A, Amikura R, Mukai M, Kobayashi S, Lasko P. Requirement for a noncoding RNA in *Drosophila* polar granules for germ cell establishment. Science. 1996;274:2075-9.

43. Gavis ER, Lunsford L, Bergsten SE, Lehmann R. A conserved 90 nucleotide element mediates translational repression of *nanos* RNA. Development. 1996;122:2791-800.

44. Gorlach J, Fox DS, Cutler NS, Cox GM, Perfect JR, Heitman J. Identification and characterization of a highly conserved calcineurin binding protein, CBP1/calcipressin, in *Cryptococcus neoformans*. EMBO J. 2000;19(14):3618-29. doi: 10.1093/emboj/19.14.3618. PubMed PMID: 10899116; PubMed Central PMCID: PMCPMC313974.

45. Kingsbury TJ, Cunningham KW. A conserved family of calcineurin regulators. Genes Dev. 2000;14(13):1595-604. PubMed PMID: 10887154; PubMed Central PMCID: PMCPMC316734.

46. Lee JI, Dhakal BK, Lee J, Bandyopadhyay J, Jeong SY, Eom SH, et al. The *Caenorhabditis elegan*s homologue of Down syndrome critical region 1, RCN-1, inhibits multiple functions of the phosphatase calcineurin. J Mol Biol. 2003;328(1):147-56. doi: 10.1016/s0022-2836(03)00237-7. PubMed PMID: 12684004.

47. Fuentes JJ, Genesca L, Kingsbury TJ, Cunningham KW, Perez-Riba M, Estivill X, et al. DSCR1, overexpressed in Down syndrome, is an inhibitor of calcineurin-mediated signaling pathways. Hum Mol Genet. 2000;9(11):1681-90. doi: 10.1093/hmg/9.11.1681. PubMed PMID: 10861295.

48. Kaneuchi T, Sartain CV, Takeo S, Horner VL, Buehner NA, Aigaki T, et al. Calcium waves occur as *Drosophila* oocytes activate. Proc Natl Acad Sci U S A. 2015;112(3):791-6. Epub 20150106. doi: 10.1073/pnas.1420589112. PubMed PMID: 25564670; PubMed Central PMCID: PMCPMC4311822.

49. Buchman AB, Brogan DJ, Sun R, Yang T, Hsu PD, Akbari OS. Programmable RNA Targeting Using CasRx in Flies. CRISPR J. 2020;3(3):164-76. Epub 2020/06/26. doi: 10.1089/crispr.2020.0018. PubMed PMID: 32584145; PubMed Central PMCID: PMCPMC7307691.

50. Tsai FC, Seki A, Yang HW, Hayer A, Carrasco S, Malmersjo S, et al. A polarized Ca2+, diacylglycerol and STIM1 signalling system regulates directed cell migration. Nat Cell Biol. 2014;16(2):133-44. Epub 20140126. doi: 10.1038/ncb2906. PubMed PMID: 24463606; PubMed Central PMCID: PMCPMC3953390.

51. Lawson MA, Maxfield FR. Ca(2+)- and calcineurin-dependent recycling of an integrin to the front of migrating neutrophils. Nature. 1995;377(6544):75-9. doi: 10.1038/377075a0. PubMed PMID: 7544874.

52. Villalobo A, Berchtold MW. The role of calmodulin in tumor cell migration, invasiveness, and metastasis. Int J Mol Sci. 2020;21(3). Epub 20200124. doi: 10.3390/ijms21030765. PubMed PMID: 31991573; PubMed Central PMCID: PMCPMC7037201.

53. Kashyap T, Rabinovitz I. The calcium/calcineurin pathway promotes hemidesmosome stability through inhibition of beta4 integrin phosphorylation. J Biol Chem. 2012;287(39):32440-9. Epub 20120803. doi: 10.1074/jbc.M112.385245. PubMed PMID: 22865863; PubMed Central PMCID: PMCPMC3463366.

54. Liu Y, Zhang Y, Min J, Liu LL, Ma NQ, Feng YM, et al. Calcineurin promotes proliferation, migration, and invasion of small cell lung cancer. Tumour Biol. 2010;31(3):199-207. Epub 20100427. doi: 10.1007/s13277-010-0031-y. PubMed PMID: 20422345.

55. Wallingford JB, Ewald AJ, Harland RM, Fraser SE. Calcium signaling during convergent extension in Xenopus. Curr Biol. 2001;11(9):652-61. doi: 10.1016/s0960-9822(01)00201-9. PubMed PMID: 11369228.

56. Takano K, Obata S, Komazaki S, Masumoto M, Oinuma T, Ito Y, et al. Development of Ca(2)(+) signaling mechanisms and cell motility in presumptive ectodermal cells during amphibian gastrulation. Dev Growth Differ. 2011;53(1):37-47. doi: 10.1111/j.1440-169X.2010.01220.x. PubMed PMID: 21261609.

57. Hayashi K, Yamamoto TS, Ueno N. Intracellular calcium signal at the leading edge regulates mesodermal sheet migration during Xenopus gastrulation. Sci Rep. 2018;8(1):2433. Epub 20180205. doi: 10.1038/s41598-018-20747-w. PubMed PMID: 29402947; PubMed Central PMCID: PMCPMC5799360.

58. Wessels HH, Mendez-Mancilla A, Guo X, Legut M, Daniloski Z, Sanjana NE. Massively parallel Cas13 screens reveal principles for guide RNA design. Nat Biotechnol. 2020;38(6):722-7. Epub 20200316. doi: 10.1038/s41587-020-0456-9. PubMed PMID: 32518401; PubMed Central PMCID: PMCPMC7294996.

59. Guo X, Rahman JA, Wessels HH, Mendez-Mancilla A, Haro D, Chen X, et al. Transcriptome-wide Cas13 guide RNA design for model organisms and viral RNA pathogens. Cell Genom. 2021;1(1). Epub 20210903. doi: 10.1016/j.xgen.2021.100001. PubMed PMID: 35664829; PubMed Central PMCID: PMCPMC9164475.

60. Ashburner M. *Drosophila*: a laboratory manual. Cold Spring Harbor: Cold Spring Harbor Press; 1989.

61. Eichler CE, Hakes AC, Hull B, Gavis ER. Compartmentalized *oskar* degradation in the germ plasm safeguards germline development. Elife. 2020;9:e49988. Epub 2020/01/08. doi: 10.7554/eLife.49988. PubMed PMID: 31909715; PubMed Central PMCID: PMCPMC6986870.

62. Wieschaus EF, Nüsslein-Volhard C. Looking at embryos. In: Roberts DB, editor. *Drosophila*: A Practical Approach. Oxford: IRL Press; 1986. p. 199-227.

63. Livak KJ, Schmittgen TD. Analysis of relative gene expression data using real-time quantitative PCR and the 2(-Delta Delta C(T)) Method. Methods. 2001;25(4):402-8. doi: 10.1006/meth.2001.1262. PubMed PMID: 11846609.